HIGH PERFORMANCE CONTROLLERS BASED ON REAL PARAMETERS TO ACCOUNT FOR PARAMETER VARIATIONS DUE TO IRON SATURATION

Jorge G. Cintron-Rivera[1], Ph.D. Candidate
Shanelle N. Foster[1], Ph.D. Candidate
Wesley G. Zanardelli[2], Ph.D.
and Elias G. Strangas[1], Ph.D.
[1]Michigan State University -Department of ECE - East Lansing, MI 48824
[2]Advanced Propulsion - U.S. ARMY TARDEC - Warren, MI 48397

ABSTRACT

With the increase in electric power on military ground vehicle platforms, electrically driven accessories are replacing existing hydraulic, belt, and gear-driven loads. Permanent Magnet Synchronous Machines (PMSM) are often selected to drive these accessories, and are under consideration for the main engine generator, due to their torque density and efficiency being among the highest available. To maximize the efficiency of a PMSM, accurate knowledge of its parameters is required across the entire operating range. Efficient control of the onboard electric drives will help reduce fuel consumption in the ground vehicle fleet. This paper presents the effects of iron saturation on the performance of a PMSM drive. Iron saturation depends on the amount of current injected into the motor and it restricts the amount of flux linkage that can be generated. PMSMs are controlled using a two axis space vector representation. Ideally, the control is decoupled, such that the flux linkage production in one axis is not affected by the current in the other axis. However, iron saturation alters this behavior and the flux linkages become dependent on both axis currents. This paper demonstrates this phenomenon by parametric experimental characterization of two permanent magnet synchronous motors. A simple but dependable method to approximate and include all the saturation effects, based on real parameters, is proposed. The effectiveness of the proposed method is validated through a simulation using the experimentally extracted parameters.

INTRODUCTION

Future Army ground vehicle platforms are expected to generate significantly greater levels of onboard electric power, [1]. While traditional alternators can source approximately 600A current at 28VDC (16.8kW), emerging high-voltage generators directly driven by the engine's crankshaft can produce nearly an order-of-magnitude increase in electric power (125-160kW). Benefits of the increased electric power include greater electrification of vehicle loads and intelligent power management, including some of the most significant loads such as the main engine cooling fan(s) and air conditioning compressor. A key challenge remains to ensure that these loads along with the generator operate at maximum efficiency, [2].

Instead of being driven through a set of gears, a belt drive, or a hydraulic system, electrified accessories lend themselves well to variable speed operation and intelligent power management strategies, [3]-[5]. This allows them to run at varying operating points regardless of the main engine speed and they can be power limited on demand to support higher priority loads. While electric drives are generally able to efficiently convert electrical to mechanical power bi-directionally, there are still opportunities to further improve this conversion efficiency, reducing the overall thermal burden on the vehicle cooling system.

The key to improving the performance and efficiency of a motor drive is to develop controllers based on real parameters, [6]-[7]. Such controllers are capable of acknowledging the parameters' non-ideal behaviors and using them to operate as efficiently as possible, [8].

In [9], a look-up table to implement Maximum Torque Per Amp (MTPA) control is proposed. This method does not

		Form Approved
Report Documentation Page		*OMB No. 0704-0188*

1. REPORT DATE **25 JUL 2013**	2. REPORT TYPE **Journal Article**	3. DATES COVERED **10-04-2013 to 15-07-2013**
4. TITLE AND SUBTITLE **HIGH PERFORMANCE CONTROLLERS BASED ON REALPARAMETERS TO ACCOUNT FOR PARAMETER VARIATIONS DUE TO IRON SATURATION**		5a. CONTRACT NUMBER
		5b. GRANT NUMBER
		5c. PROGRAM ELEMENT NUMBER
6. AUTHOR(S) **Jorge Cintron-Rivera; Shanelle Foster; Wesley Zanardelli; Elias Strangas**		5d. PROJECT NUMBER
		5e. TASK NUMBER
		5f. WORK UNIT NUMBER
7. PERFORMING ORGANIZATION NAME(S) AND ADDRESS(ES) **Michigan State University,Department of ECE,426 Auditorium Rd,East Lansing,Mi,48824**		8. PERFORMING ORGANIZATION REPORT NUMBER **; #24051**
9. SPONSORING/MONITORING AGENCY NAME(S) AND ADDRESS(ES) **U.S. Army TARDEC, 6501 East Eleven Mile Rd, Warren, Mi, 48397-5000**		10. SPONSOR/MONITOR'S ACRONYM(S) **TARDEC**
		11. SPONSOR/MONITOR'S REPORT NUMBER(S) **#24051**

12. DISTRIBUTION/AVAILABILITY STATEMENT
Approved for public release; distribution unlimited

13. SUPPLEMENTARY NOTES
GROUND VEHICLE SYSTEMS ENGINEERING AND TECHNOLOGY SYMPOSIUM (GVSETS), SET FOR AUG. 21-22, 2013

14. ABSTRACT

With the increase in electric power on military ground vehicle platforms, electrically driven accessories are replacing existing hydraulic, belt, and gear-driven loads. Permanent Magnet Synchronous Machines (PMSM) are often selected to drive these accessories, and are under consideration for the main engine generator, due to their torque density and efficiency being among the highest available. To maximize the efficiency of a PMSM, accurate knowledge of its parameters is required across the entire operating range. Efficient control of the onboard electric drives will help reduce fuel consumption in the ground vehicle fleet. This paper presents the effects of iron saturation on the performance of a PMSM drive. Iron saturation depends on the amount of current injected into the motor and it restricts the amount of flux linkage that can be generated. PMSMs are controlled using a two axis space vector representation. Ideally, the control is decoupled, such that the flux linkage production in one axis is not affected by the current in the other axis. However, iron saturation alters this behavior and the flux linkages become dependent on both axis currents. This paper demonstrates this phenomenon by parametric experimental characterization of two permanent magnet synchronous motors. A simple but dependable method to approximate and include all the saturation effects, based on real parameters, is proposed. The effectiveness of the proposed method is validated through a simulation using the experimentally extracted parameters.

15. SUBJECT TERMS

16. SECURITY CLASSIFICATION OF:			17. LIMITATION OF ABSTRACT	18. NUMBER OF PAGES	19a. NAME OF RESPONSIBLE PERSON
a. REPORT **unclassified**	b. ABSTRACT **unclassified**	c. THIS PAGE **unclassified**	**Public Release**	**9**	

include saturation effects. PMSMs are usually operated under saturation [10], neglecting these effects can lead to controller performance degradation [11].

All saturation effects were included in both controllers proposed in [12] and [13]. In [12], signal injection was used to determine the parameters needed to develop lookup tables and in [13], finite element analysis was used to identify the machine parameters. Neither controller, however, is capable of operating in the field weakening region.

In this paper, a method to approximate the parameters of a PMSM is proposed. The method is based on experimental data and it includes the saturation effects using piecewise linear functions. The method was validated, in the MTPA and field weakening regions, using simulations based on real parameters from two 125kW PMSMs.

BACKGROUND THEORY AND MODELING

Permanent magnet synchronous machines are modeled using the equivalent two axis model shown in Figure 1, referred to as the synchronous frame of reference. This model is obtained by applying the Park's transformation matrix to the three phase stator quantities.
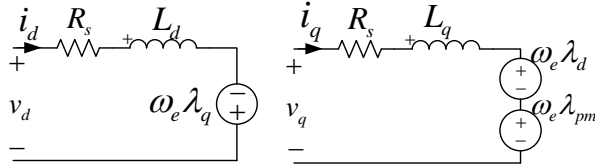

Figure 1: Equivalent two axes model for a PMSM.

The complete machine model after Park's transformation is given by equations (1) - (5).

$$v_d = R_s i_d + L_d \frac{di_d}{dt} - \omega_e L_q i_q = R_s i_d + \frac{d\lambda_d}{dt} - \omega_e \lambda_q \quad (1)$$

$$v_q = R_s i_q + L_q \frac{di_q}{dt} + \omega_e \lambda_d = R_s i_q + \frac{d\lambda_q}{dt} + \omega_e \lambda_d \quad (2)$$

$$\lambda_d = L_d i_d + \lambda_{pm} \quad (3)$$
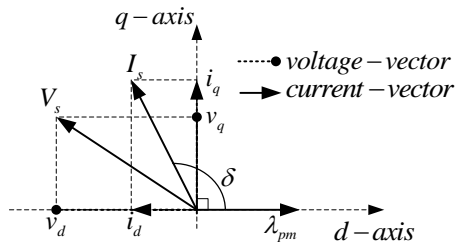
$$\lambda_q = L_q i_q \quad (4)$$

Figure 2: Vector orientation used for model development and control techniques.

$$T = \frac{3P}{4} \left\{ \lambda_d i_q - \lambda_q i_d \right\} \quad (5)$$

Where, i_d, i_q, v_d and v_q are the currents and voltages in the direct and quadrature axes. λ_{pm}, λ_d and λ_q are the flux linkages due to the permanent magnets and the corresponding axes currents. L_d and L_q are the direct and quadrature axis inductances, ω_e is the electrical speed of the motor and T is torque

Figure 2 shows the orientation frame to which the motor model, (1)-(5), is referred. In this orientation, the flux linkage due to the magnets lies on the positive d-axis, and torque is only produced by the quadrature current. The direct axis current is used as a field weakening mechanism and in the case of an interior permanent magnet machine it enables the production of reluctance torque. For motoring, PMSMs are generally operated in the second quadrant of the space plane, Figure 2, to perform field weakening and develop the magnetic and reluctance torques.

This classical model (1)-(5) is based on ideal conditions where the effects of iron losses, self and cross saturation, are neglected. To study the effects of losses and iron saturation in PMSMs the classical model is extended in order to include these effects.

When i_d and i_q saturate the iron paths in each corresponding axis, the flux linkages produced by the magnetizing currents are no longer decoupled as shown in the ideal model (3) and (4). Instead, the flux linkages become coupled to both axis currents, this coupling effect can be modeled as follows,

$$\lambda_d \left(i_d, i_q \right) = L_d(i_d) i_d + L_{dq}(i_d, i_q) i_q + \lambda_{pm} \quad (6)$$

$$\lambda_q \left(i_d, i_q \right) = L_q(i_q) i_q + L_{qd}(i_d, i_q) i_d \quad (7)$$

where, $L_d(i_d)$ and $L_q(i_q)$ are the baseline inductances for each of the axes. They represent the corresponding axis self-inductance as a function of the axis current and are calculated assuming no cross saturation from the other-axis current, [6]. $L_{dq}(i_d, i_q)$ and $L_{qd}(i_d, i_q)$ are the cross
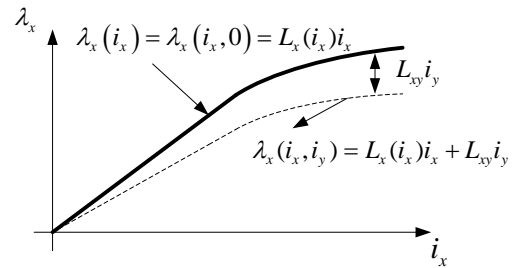

Figure 3: Self and cross saturation of the flux linkages

HIGH PERFORMANCE CONTROLLERS BASED ON REAL PARAMETERS TO ACCOUNT FOR PARAMETER VARIATIONS DUE TO IRON SATURATION

coupling inductances for each axis and add the cross saturation effects to the machine model. This self and cross saturation behavior is illustrated in Figure 3, where the x and y variables represent the d and q-axis

Equations (6) and (7) could be written in a variety of ways to model the effect of both currents on the d and q-axis fluxes. The formulation used in this paper assigns all the cross coupling to the quasi-mutual inductances L_{dq} and L_{qd}, the rest of the saturation to L_d and L_q, and assumes no effect of saturation of the flux due to magnets, without decreasing the model accuracy.

The machine model including the saturation effects is calculated by substituting (6) and (7) into (1)-(5). After some algebraic manipulation, the modified machine model is given by (8)-(10).

$$v_d = R_s i_d + \left[L_d(i_d)\frac{di_d}{dt} + L_{dq}(i_d,i_q)\frac{di_q}{dt} \right]$$
$$-\omega_e \left\{ L_q(i_q)i_q + L_{qd}(i_d,i_q)i_d \right\} \tag{8}$$

$$v_q = R_s i_q + \left[L_q(i_q)\frac{di_q}{dt} + L_{qd}(i_d,i_q)\frac{di_d}{dt} \right]$$
$$+\omega_e \left\{ L_d(i_d)i_d + L_{dq}i_q(i_d,i_q) + \lambda_{pm} \right\} \tag{9}$$

$$T = \frac{3P}{4}\left\{ \lambda_d\left(i_d,i_q\right)i_q - \lambda_q\left(i_d,i_q\right)i_d \right\} \tag{10}$$

PARAMETER IDENTIFICATION PROCESS

This paper is aimed to find and quantify the PMSM parameters, including the self and cross saturation effects, in order to develop a high performance controller. Knowledge of the non-ideal parameters is essential to develop a highly efficient motor drive, [10].

To quantify this behavior, the parameter identification method proposed in [6] was used. This method is capable of extracting the parameters, including the non-ideal characteristics, by collecting and processing experimental data. Similar methods for parametric identification have been proposed, [7] and they follow the same characterization principle.

The identification process is divided into two main procedures: Experimental data collection, as shown in Figure 4, and off-line data processing. During the characterization process, the machine is studied over its entire current operating range. The experimental data is obtained at a particular speed, and all possible current and angle combinations are applied to the machine. At every current/angle combination, the phase voltage information, experimental line currents, and rotor position are recorded. Then, this information is processed off-line to accurately determine the machine flux linkages, $\lambda_d(i_d,i_q)$ and
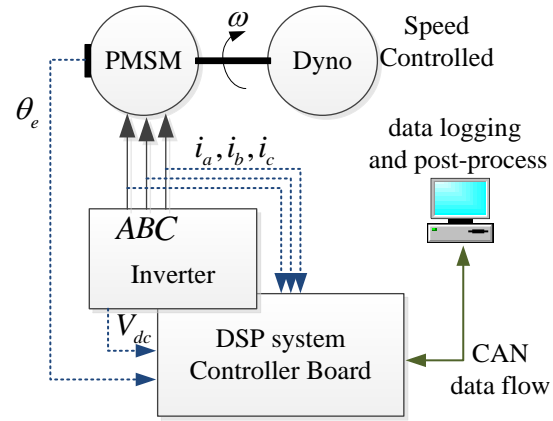

Figure 4: Experimental Setup

$\lambda_q(i_d,i_q)$, using (11) and (12). Given that the information collected comes from experimental data, the saturation effects and nonlinear behavior of the PMSM are captured.

$$\lambda_d\left(i_d,i_q\right) = \frac{v_q - i_q R_s}{\omega_e} \tag{11}$$

$$\lambda_q\left(i_d,i_q\right) = \frac{i_d R_s - v_d}{\omega_e} \tag{12}$$

The flux information obtained is sufficient to develop a high performance controller, since $\lambda_d(i_d,i_q)$ and $\lambda_q(i_d,i_q)$ include the non-ideal characteristics of the machine. The non-ideal inductance values can be calculated from this information.

EXPERIMENTAL CHARACTERIZATION

Two PMSMs, a motor and a generator, were characterized in order to study the effects of iron saturation. The characteristics for each machine are given in table 1.

Parameters	Motor	Generator
Rated power	125 kW	125 kW
Rated speed	1500 RPM	1900 RPM
Max speed	5000 RPM	3000 RPM
Line voltage	480 V_{LL}	480 V_{LL}
Max current	250 A_{peak}	250 A_{peak}
No. poles	4	8

Table 1: PMSM parameters

The parameters for both machines were determined at 700 RPM as shown in figures 5-8. This speed is sufficient to generate a measurable back-EMF voltage and it is below the base speed. Therefore, it is possible to collect experimental data for all the rated current combinations of i_d and i_q.

HIGH PERFORMANCE CONTROLLERS BASED ON REAL PARAMETERS TO ACCOUNT FOR PARAMETER VARIATIONS DUE TO IRON SATURATION

The experimental results in Figures 5-8, demonstrate that self and cross-saturation are non-ideal characteristics that cannot be ignored or assumed to be negligible. For the motor, the flux linkage along the *d*-axis had as much as 38.5% variation due to cross saturation, while the *q*-axis had as much as 23.7% variation.

The generator behavior is similar, with flux variations as high as 31.4% on the *d*-axis flux and 14.5% on the *q*-axis due to cross saturation. These non-ideal parametric variations have a negative impact on the torque production of the machine, since the torque is directly proportional to the flux linkages, as shown in (10). Efficiency is also affected, as the parametric variations will detune the motor controller. For a given operating condition, the controller will not inject the optimal currents to generate the desired torque.
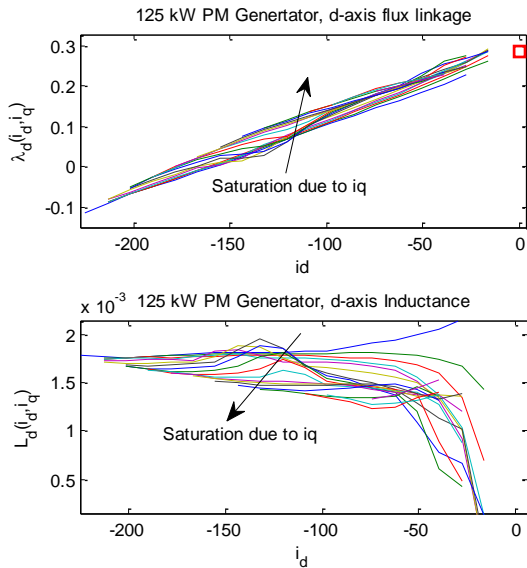
Figure 5: Generator experimentally extracted d-axis flux linkage and d-axis inductance.
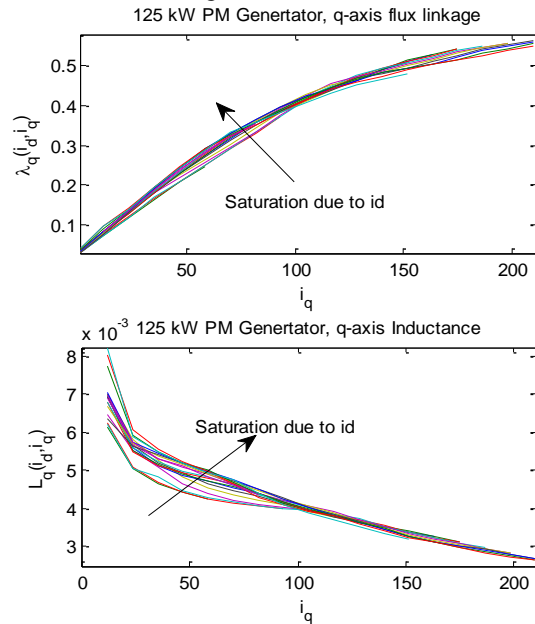
Figure 6: Generator experimentally extracted q-axis flux linkage and q-axis inductance.
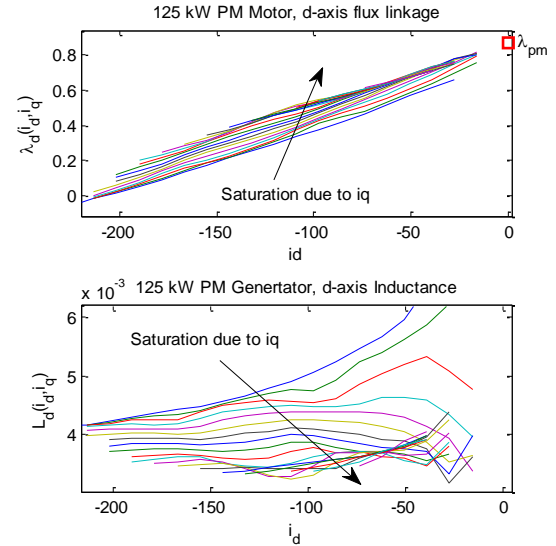
Figure 7: Motor experimentally extracted d-axis flux linkage and d-axis inductance.
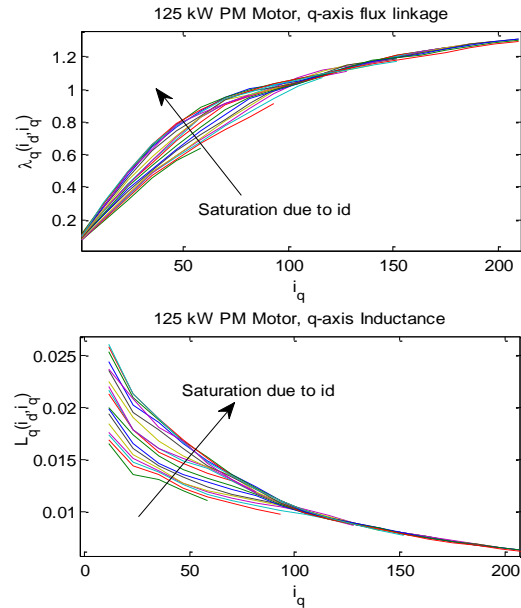
Figure 8: Motor experimentally extracted q-axis flux linkage and q-axis inductance.

HIGH PERFORMANCE CONTROLLERS BASED ON REAL PARAMETERS TO ACCOUNT FOR PARAMETER VARIATIONS DUE TO IRON SATURATION

Both machines were also characterized through Finite Element Analysis (FEA). FEA is an excellent tool to determine the basic operating characteristic of a PMSM. It is capable of including both self- and cross-saturation effects. However, the inclusion of cross-saturation effects with FEA requires lengthy calculation time and a transient-magnetic simulation.

Figure 9 and 10 show the axis inductances for each machine, determined using a FEA Magneto-static simulation scenario. This type of simulation was used, since it is considerably less time consuming than a full transient-magnetic simulation. These inductances fit within the experimental inductances shown in Figures 5-8.
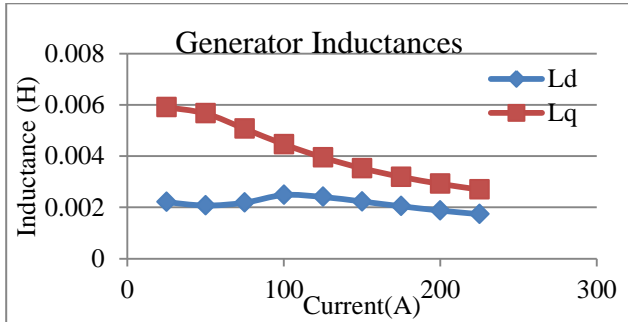

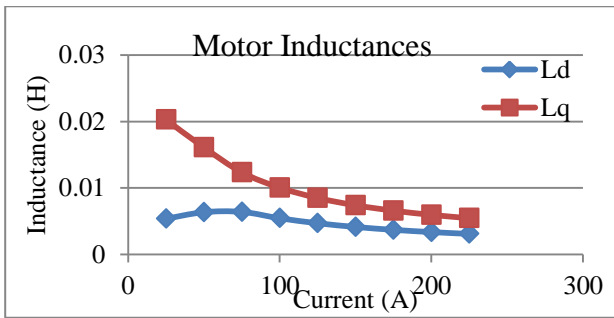**Figure 9:** Generator Finite Element Analysis d- and q-axis inductance.

Figure 10: Motor Finite Element Analysis d- and q-axis inductance.

PROPOSED PARAMETER APPROXIMATION

In order to develop a high performance controller, accurate knowledge of the parameters is required across the entire operating range. Look Up Tables (LUTs) are commonly used to develop controllers based on real parameters. By using a controller based on a LUT, it is possible to fully include the non-ideal parameter behavior shown in Figures 5-8 in the motor controller.

The main drawback of a LUT is the required memory in the controller. The memory space requirement is directly proportional to the resolution of the LUT, [14]. In many applications, Digital Signal Processors (DSPs) are used to

implement the controller. These DSPs are commercially fabricated with a limited memory capacity. A LUT can be implemented in a DSP controller; however, the LUT resolution must be reduced to fit it in the available memory. This can lead to a decrease in performance of the controller, as information is removed from the table's entries.

An accurate curve-fit method to approximate the real parameters of the motor and generator is proposed in this paper. The method is a dynamic piecewise linear approximation that includes the parameters' non-ideal characteristics, i.e., the cross-saturation effect. It can perform as well as a full parametric LUT controller, but it will not overstress the DSP/microcontroller memory, nor consume much computation time.

For the case of $L_d(i_d, i_q)$, the true inductance, shown in Figures 5 and 7, is divided into two linear sectors, as shown in Figure 11. The first step is to determine the baseline d-axis inductance from the experimental data, given by (13).

$$L_d(i_d, i_q)\Big|_{i_q = 0} = L_d(i_d, 0) \qquad (13)$$

The two linear approximations for (13) are highlighted in Figure 11 by the line with stars markers. Finally, the cross saturation for this case is added by subtracting from this baseline approximation, as the other axis current increases. It is assumed that cross-saturation in the d-axis increases linearly with the q-axis current. The incremental function is defined as $\Lambda(i_q)$. By using the experimental data and inspection, it is determined that the function representing the cross-saturation terms is as shown in (14). Finally, the total inductance in these two sectors is given by equation (15).
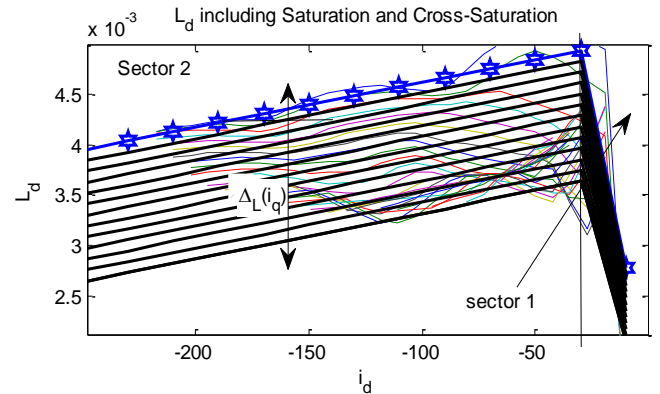

Figure 11: Motor d-axis inductance piecewise linear approximation, including cross saturation.

$$\Lambda_d^{sec1\&2}(i_q) = \frac{-\Delta_L(i_q)}{i_{rated}} i_q \qquad (14)$$

$$L_d(i_d, i_q) = L_d(i_d) + \Lambda_d^{sec1\&1}(i_q) \qquad (15)$$

HIGH PERFORMANCE CONTROLLERS BASED ON REAL PARAMETERS TO ACCOUNT FOR PARAMETER VARIATIONS DUE TO IRON SATURATION

In Figure 11, the two sector linear approximation and the true experimental inductances are plotted together to illustrated the approximation usefulness.

The *q*-axis inductance requires more linear sectors, as shown in Figures 6 and 8, since it suffers higher saturation than the *d*-axis quantities. Instead of two sectors to approximate this inductance, four sectors are used as shown in Figure 12.

The linear approximations made in each sector are discussed from right to left, beginning with sector 4. As shown in Figures 6 and 8, the effect from the *d*-axis current is minimal in this sector. Therefore, the inductance approximation is made by finding the linear equation that intersects points ζ_4 and ζ_5.
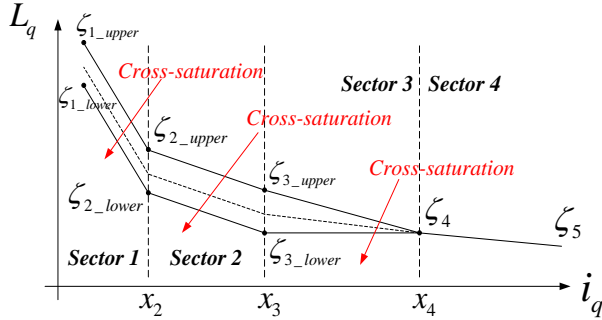

Figure 12: *q*-axis inductance piecewise linear approximation, including cross saturation in four sectors.

In sector 3, the cross-saturation effects are added by introducing a dynamic slope change. In this sector, ζ_4 is a fixed point, but the slope of the baseline inductance is adjusted as a linear function of i_d, given by $\widetilde{m}(i_d)$. The expressions to determine the *q*-axis inductance in sector 3 are given by (16)-(18).

$$m(i_d) = \frac{\zeta_{3\_lower} - \zeta_{3\_upper}}{i_{d\_rated} \cdot (x_4 - x_3)} \cdot i_d + \frac{\zeta_4 - \zeta_{3\_upper}}{x_4 - x_3} \quad (16)$$

$$\Lambda_d^{sec.3}(i_d) = \frac{\zeta_{3\_upper} - \zeta_{3\_lower}}{i_{rated}} \cdot i_d + \zeta_{3\_upper} \quad (17)$$

$$L_q(i_d, i_q)\Big|_{sec.3} = m(i_d) \cdot (i_q - x_3) + \Lambda_d^{sec.3}(i_d) \quad (18)$$

In sectors 2 and 1, the linear approximation is made using the same technique used for the *d*-axis inductance, where the slope is constant and the cross-saturation is modeled by the linear function $\Lambda_q^{sec.2\&1}(i_d)$. Note that all values of ζ are known from the experimental data. The complete approximation for the motor *q*-axis inductance along with the true experimental values are shown in Figure 13.

The inductance approximations for the generator were determined using the same technique and the results are similar to those of the motor.
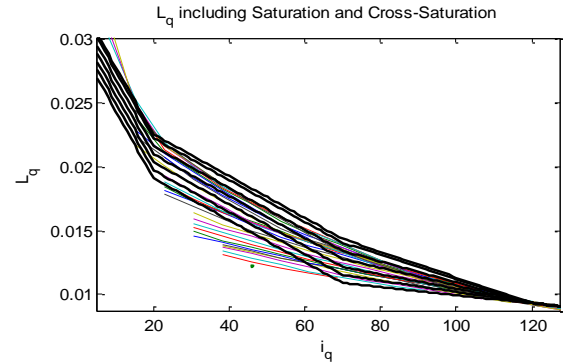

Figure 13: Motor *d*-axis inductance piecewise linear approximation on top of the experimental *q*-axis inductance.

CONTROLLER PERFORMANCE EVALUATION

To evaluate the accuracy of the proposed parameter approximation method, a performance simulation based on experimental data was developed for each PMSM. The simulation was performed with four different controllers as shown in Figure 14. For this study, only the copper losses were considered. This leads to high efficiency results, but it serves as a proof of concept.
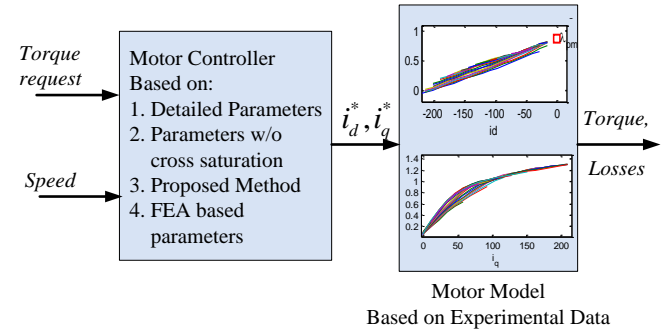

F**igure 14**: Simulation based on motor experimental data.

First, a highly detailed controller was developed using a LUT. This controller contains all the saturation effects of the motor. Therefore, this controller is used as the baseline. The tables' resolution has steps of 2.5A from zero to 250A. For each current step there is a table entry that matches a torque command and a speed to a set of i_d and i_q.

The second controller was developed using experimental data, but the cross-saturation effects were ignored. For this case the table's resolution is the same as the first case. The third controller is developed using the proposed parameter approximation method. Finally, a controller based on FEA was developed to compare with the experimental

HIGH PERFORMANCE CONTROLLERS BASED ON REAL PARAMETERS TO ACCOUNT FOR PARAMETER VARIATIONS DUE TO IRON SATURATION

parameters. The controllers developed using the proposed and FEA parameters are based on curve fit methods.

Each controller was tested in the MTPA and field-weakening regions. For each region, the torque command was varied from 200 Nm to maximum, and the power copper losses and torque for each operating point was calculated. The results for the performance simulation are shown in Figures 15-18.
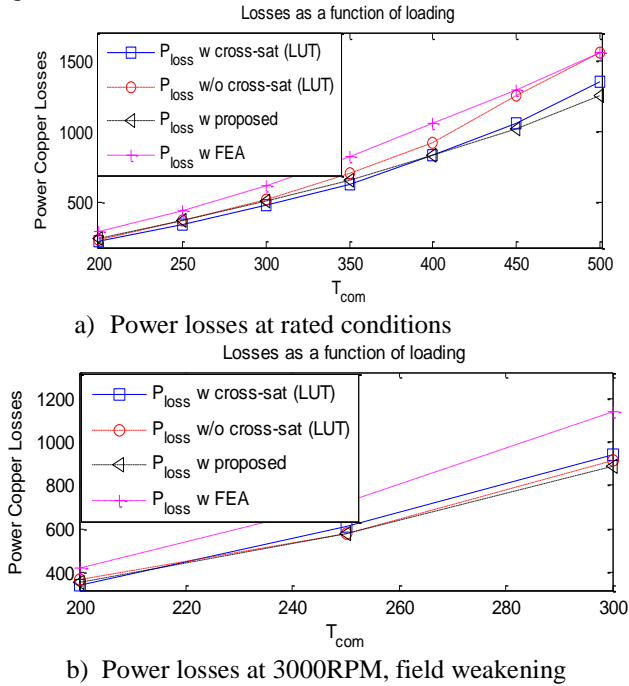

a) Power losses at rated conditions

b) Power losses at 3000RPM, field weakening

Figure 15: Generator P_{losses} (considering copper losses only), at a) rated conditions, and b) a deep field weakening operation point.
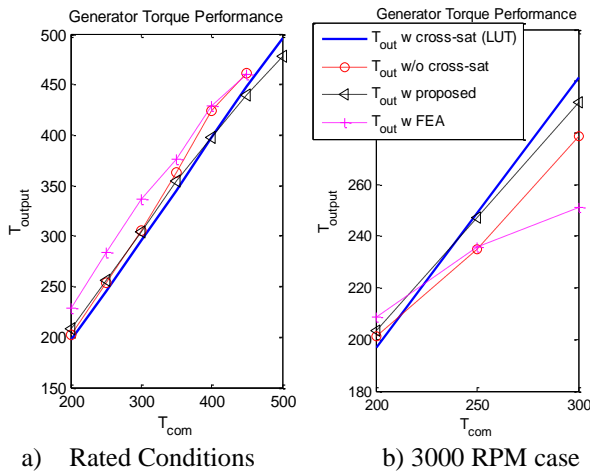

a) Rated Conditions   b) 3000 RPM case

Figure 16: Generator torque (considering copper losses only), at a) rated conditions, and b) a deep field weakening operation point.

Figures 15 and 16 show the performance simulation for the generator. For both operating regions, the controller that performed almost as well as the baseline high resolution LUT controller was the controller designed with the proposed parameter approximation method. This statement is based on the lower power losses and the torque tracking effectiveness.

Figure 15 shows that minimum power losses were achieved with the base line controller and the controller using the proposed parameters' approximation technique. On the other hand, the controllers designed using FEA parameters and the parameters ignoring cross-saturation are the controllers that yielded the highest power losses. Similar behavior was noted for the torque performance shown in Figure 16 where the controller designed using the proposed parameters follows the detailed LUT controller torque performance.
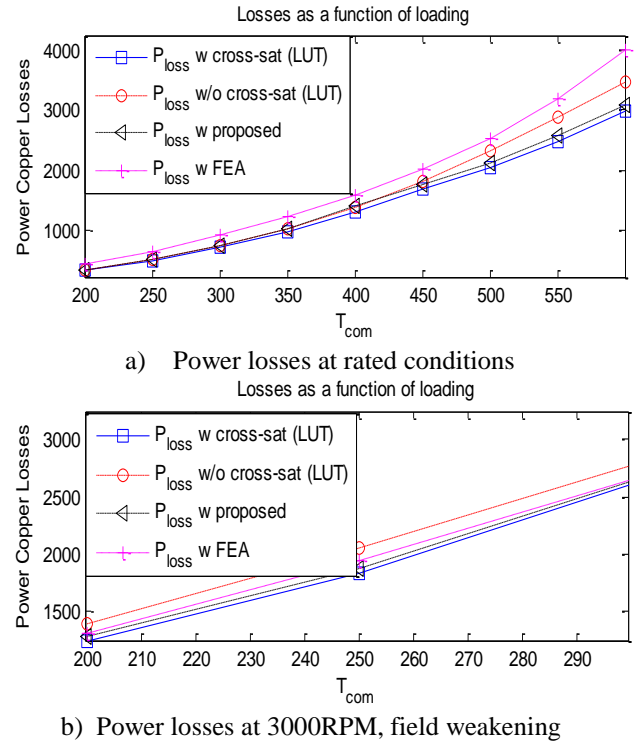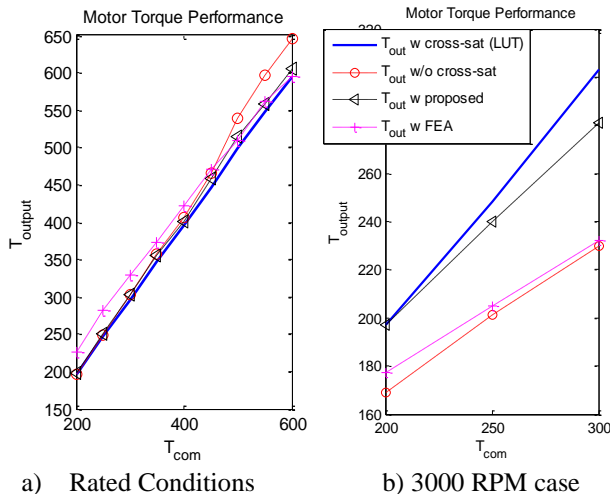

a) Power losses at rated conditions

b) Power losses at 3000RPM, field weakening

Figure 17: Motor P_{losses} (considering copper losses only), at a) rated conditions, and b) a deep field weakening operation point.

The motor exhibited similar behavior as shown in Figures 17 and 18. However, power losses are higher for the motor because it experiences more cross-saturation than the generator. For the motor, the controller designed using the proposed parameter approximation method had the closest performance to the detailed LUT controller.

HIGH PERFORMANCE CONTROLLERS BASED ON REAL PARAMETERS TO ACCOUNT FOR PARAMETER VARIATIONS DUE TO IRON SATURATION

a)   Rated Conditions   b) 3000 RPM case

Figure 18: Motor torque (considering copper losses only), at a) rated conditions, and b) a deep field weakening operation point.

CONCLUSIONS

In this paper, the effects of iron saturation on the performance of a motor drive are studied using two PMSMs. The flux linkages and inductances of each machine were determined through a characterization process and are shown in Figures 5-8. Saturation is evident from these figures and cannot be ignored or assumed negligible.

It is possible to obtain the parameters required to design a motor controller through FEA simulations or experimental data collection. The inclusion of cross-saturation effects in the controller development is vital to ensure a high performance, high efficiency controller.

A method to include these effects is proposed. It was tested against controllers based on high resolution LUT, LUT without cross-saturation, and FEA parameters. Figures 15-18 demonstrate the validity of the method. The simulations showed that the proposed method has low P_{losses} and good torque performance; both metrics are comparable to the performance of the high resolution LUT controller at both low and high speeds.

Compared with conventional approaches, the proposed method applied to a 125kW machine contributed to a reduction in copper losses as high as 900W, resulting in an efficiency gain of 1.36%. The proposed controller, incorporating a dynamic piecewise linear approximation of the machine flux linkages, is realizable in the majority of motor control DSPs used in high performance PMSM controllers due to its computational efficiency.   The controller helps to improve the dynamic response of the drive and its improved efficiency contributes to a decreased thermal burden on the cooling system in military ground vehicle applications.

REFERENCES

[1] Khalil, G., "Challenges of hybrid electric vehicles for military applications," Vehicle Power and Propulsion Conference, 2009. VPPC '09. IEEE , vol., no., pp.1,3, 7-10 Sept. 2009

[2] Yuan Cheng; Trigui, R.; Espanet, C.; Bouscayrol, A.; Shumei Cui, "Specifications and Design of a PM Electric Variable Transmission for Toyota Prius II," Vehicular Technology, IEEE Transactions on , vol.60, no.9, pp.4106,4114, Nov. 2011

[3] Estima, J.O.; Marques Cardoso, A.J., "Efficiency Analysis of Drive Train Topologies Applied to Electric/Hybrid Vehicles," Vehicular Technology, IEEE Transactions on , vol.61, no.3, pp.1021,1031, March 2012

[4] Seok-Myeong Jang; Seon-Ik Hwang; Kyoung-Jin Ko; Jang-Young Choi; So-Young Sung, "Driving performance evaluation of interior permanent magnet (IPM) motor using circuit parameter estimation," Electrical Machines and Systems (ICEMS), 2010 International Conference on , vol., no., pp.1205,1208, 10-13 Oct. 2010

[5] Fajkus, P.; Klima, B.; Hutak, P., "High speed range field oriented control for permanent magnet synchronous motor," Power Electronics, Electrical Drives, Automation and Motion (SPEEDAM), 2012 International Symposium on , vol., no., pp.225,230, 20-22 June 2012

[6] J. G. Cintron-Rivera, A. S. Babel, E. E. Montalvo-Ortiz, S. N. Foster and E. G. Strangas, "A Simplified Characterization Method Including Saturation Effects for Permanent Magnet Machines," 2012 International Conference on Electrical Machines (ICEM), pp. 837-843, 2012.

[7] Babel, A.S.; Foster, S.N.; Cintron-Rivera, J.G.; Strangas, E.G., "Parametric sensitivity in the analysis and control of permanent magnet synchronous machines," Electrical Machines (ICEM), 2012 XXth International Conference on , vol., no., pp.1034,1040, 2-5 Sept. 2012

[8] S. Kim, Y. Yoon, S. Sul, K. Ide, "Maximum Torque per Ampere (MTPA) Control of an IPM Machine Based on Signal Injection Considering Inductance Saturation," Power Electronics, IEEE Transactions on , vol.28, no.1, pp.488,497, Jan. 2013.

[9] Y. Nanfang, L. Guangzhao, L. Weiguo and W. Kang, "Interior Permanent Magnet Synchronous Motor Control for Electric Vehicle Using Look-up Table," 2012 IEEE 7th International Power Electronics and

Motion Control Conference, vol. 2, pp. 1015-1019, June 2-5, 2012.

[10] T. Herold, D. Franck, E. Lange and K. Hameyer, "Extension of a d-q Model of a Permanent Magnet Excited Synchronous Machine by including Saturation, Cross-Coupling and Slotting Effects," 2011 IEEE International Electric Machines and Drives Conference (IEMDC), pp. 1363-1367, May 2011.

[11] Seok-Myeong Jang; Seon-Ik Hwang; Kyoung-Jin Ko; Jang-Young Choi; So-Young Sung, "Driving performance evaluation of interior permanent magnet (IPM) motor using circuit parameter estimation,"Electrical Machines and Systems (ICEMS), 2010 International Conference on , vol., no., pp.1205,1208, 10-13 Oct. 2010

[12] S. Kim, Y. Yoon, S. Sul, K. Ide, "Maximum Torque per Ampere (MTPA) Control of an IPM Machine Based on Signal Injection Considering Inductance Saturation," Power Electronics, IEEE Transactions on , vol.28, no.1, pp.488,497, Jan. 2013.

[13] Z. Li, H. Li, "MTPA control of PMSM system considering saturation and cross-coupling," Electrical Machines and Systems (ICEMS), 2012 15th International Conference on, vol., no., pp.1,5, 21-24 Oct. 2012

[14] J.G. Cintron-Rivera, S.N.. Foster, C.E. Nino-Baron and Elias G. Strangas, "High Performance Controllers for Interior Permanent Magnet Synchronous Machines Using Look-up Tables and Curve-fitting Methods", IEMDC 2013 Ohare, Illinois.